

# Salts of (+)-deoxycholic acid with amines: structure, thermal stability, kinetics of salt formation, decomposition and chiral resolution†

Cite this: *CrystEngComm*, 2013, 15, 931

Ayesha Jacobs,\* Nikoletta B. Báthori, Luigi R. Nassimbeni and Baganetsi K. Sebogisi

(+)-Deoxycholic acid forms salts with 1-propylamine, di-*n*-butylamine, *sec*-butylamine and 3-methyl-2-butylamine. The salts were characterised using thermal analysis and single crystal X-ray diffraction. The chiral discrimination of (+)-deoxycholic acid for racemic *sec*-butylamine and racemic 3-methyl-2-butylamine was studied and correlated with the structural and thermal results. A mixture of (+)-deoxycholic acid and racemic *sec*-butylamine yielded crystals of (*R*)-2-butylammonium deoxycholate. (+)-Deoxycholic acid was exposed to vapours of propylamine and racemic *sec*-butylamine and the kinetics of absorption were determined. The kinetics of decomposition of powdered samples obtained from (+)-deoxycholic acid with di-*n*-butylamine and racemic *sec*-butylamine were investigated. Crystallisation of (+)-deoxycholic acid with racemic 3-methyl-2-butylamine resulted in crystals of (*S*)-3-methyl-2-butylammonium deoxycholate.

Received 15th June 2012,  
Accepted 7th November 2012

DOI: 10.1039/c2ce26706c

[www.rsc.org/crystengcomm](http://www.rsc.org/crystengcomm)

## Introduction

(+)-Deoxycholic acid, **H**, is one of the important bile acids whose general formula, based on the steroid nucleus, is shown in Fig. 1, which also names some important bile acids and their substituents R1–R4 (Table 1).

Many of these acids form crystalline inclusion compounds with a variety of guests and these cholic acids have been the subject of intense structural studies since the 1930's. Deoxycholic acid (**H**) is dextro-rotatory,  $[\alpha]_D^{20} + 55^\circ$  in ethanol.<sup>1</sup> Giglio<sup>2</sup> has reviewed the inclusion compounds of **H**, their structures, lattice energies and the enthalpy changes of the guest-release reactions. Miyata<sup>3,4</sup> lists forty bile acids and their derivatives, discusses their polymorphic forms, their dynamic behaviour and reactions occurring in their channel structures. The bile acids have a rigid skeleton and their shape is characterised by a *cis*-fusion of the A and B rings, while the B, C and D rings are *trans*-fused. Hydroxyl groups point below the steroidal plane giving a hydrophilic face, while two methyl groups point above the plane, forming a lipophilic face. The side chain containing the carboxylic moiety, is flexible. All the bile acids are chiral and have been employed to resolve racemic modifications.<sup>5</sup> Recently lithocholic acid was employed to resolve *sec*-butylamine.<sup>6</sup> **H** was used in the

resolution of *erythro*-2,3-bis(*p*-methoxyphenyl)butyl- and pentyl-amines<sup>7</sup> as well as *trans*-3-amino-4-hydroxycyclopentene.<sup>8</sup> Crystallisation of **H** with racemic camphorquinone and racemic *endo*-(+)-3-bromocamphor yielded crystals of the (*S*)-enantiomers together with crystals of the racemic guests.<sup>9</sup>

The amine salts of **H**, however, have not been studied. In this work we have analysed the structures and thermal characteristics of the salts formed by **H** with the achiral guests 1-propylamine (PPA) and di-*n*-butylamine (DBA). **H** was exposed to varying vapour pressures of the guests 1-propylamine and racemic *sec*-butylamine, respectively, and the kinetics of guest absorption were analysed. The kinetics of decomposition of the salts formed by **H** with di-*n*-butylamine and racemic *sec*-butylamine were also determined. Chiral resolution *via* diastereomeric salt formation remains an important topic in chemistry,<sup>10</sup> however, the mechanism of chiral selectivity remains poorly understood. In view of this we

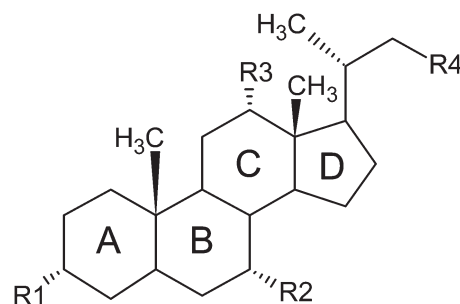


Fig. 1 General steroid structure.

Department of Chemistry, Faculty of Applied Sciences, Cape Peninsula University of Technology, PO Box 652, Cape Town 8000, South Africa.

E-mail: [jacobsa@cput.ac.za](mailto:jacobsa@cput.ac.za); Fax: +27 21 460 3854; Tel: +27 21 460 3167

† Electronic supplementary information (ESI) available: Hydrogen bond data available for all salts. CCDC 886458–886464. For ESI and crystallographic data in CIF or other electronic format see DOI: 10.1039/c2ce26706c

**Table 1** Important bile acids

R1	R2	R3	R4	Name
OH	H	H	COOH	Norlithocholic acid
OH	OH	H	COOH	Norchenodeoxycholic acid
OH	H	OH	COOH	Nordeoxycholic acid
OH	OH	OH	COOH	Norcholic acid
OH	H	H	CH <sub>2</sub> COOH	Lithocholic acid
OH	OH	H	CH <sub>2</sub> COOH	Chenodeoxycholic acid
OH	H	OH	CH <sub>2</sub> COOH	Deoxycholic acid ( <b>H</b> )
OH	OH	OH	CH <sub>2</sub> COOH	Cholic acid

have studied the chiral discrimination of **H** for racemic *sec*-butylamine (BA) and racemic 3-methyl-2-butylamine (MBA). The chiral resolution results of the two systems were correlated with the structures and thermal parameters in an effort to gain further insight into the resolution process. The atomic numbering scheme for the host and the diagram of the guests is given in Scheme 1.

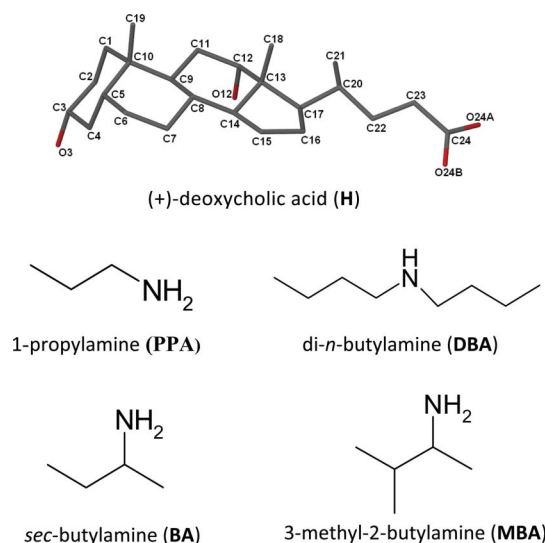
## Experimental section

### Crystal growth

(**H**<sup>−</sup>)(**PPA**<sup>+</sup>)-**ACE**: **H** was ground with a few drops of 1-propylamine. The powdered sample was dissolved in AR grade acetone (**ACE**) that had been dried using molecular sieves. The saturated solution yielded suitable crystals *via* slow evaporation.

(**2H**<sup>−</sup>)(**2PPA**<sup>+</sup>)-**4.3H**<sub>2</sub>**O** was obtained in a similar manner except the powdered sample was dissolved in undried acetone.

(**H**<sup>−</sup>)(**DBA**<sup>+</sup>) was obtained by grinding samples of **H** and drops of di-*n*-butylamine. The powder was dissolved in acetone and crystals were obtained through slow evaporation of the solution.

**Scheme 1** Atomic labelling scheme for host and schematic diagram of guests.

(**H**<sup>−</sup>)(**R-BA**<sup>+</sup>) was obtained by slow evaporation of a saturated solution of **H** in racemic *sec*-butylamine.

(**H**<sup>−</sup>)(**S-BA**<sup>+</sup>) was obtained by slow evaporation of a saturated solution of **H** in (*S*)-*sec*-butylamine.

(**H**<sup>−</sup>)(**R-MBA**<sup>+</sup>) and (**H**<sup>−</sup>)(**S-MBA**<sup>+</sup>): Powdered samples were obtained from slow evaporation of saturated solutions of **H** in the respective amine. These powders were dissolved in acetone and suitable crystals were obtained *via* slow evaporation.

### Structure analysis

Unit cell dimensions were determined from intensity data measured on Kappa CCD<sup>11</sup> and Bruker DUO APEX II<sup>12</sup> diffractometers using graphite-monochromated Mo K $\alpha$  radiation. The intensity data were collected by the standard phi scan and omega scan techniques, scaled and reduced using DENZO-SMN<sup>13</sup> or SAINT-Plus.<sup>14</sup> All of the structures were solved using direct methods and refined by full-matrix least squares with SHELX-97,<sup>15</sup> refining on *F*<sup>2</sup>. X-Seed<sup>16</sup> was used as a graphical interface. For all the structures the non-hydrogen atoms were located in difference electron density maps. The hydrogens of the host and guests not involved in hydrogen bonding were placed with geometric constraints and allowed to refine isotropically. The hydroxyl hydrogens of the host and the hydrogens attached to the nitrogen of the guests were found in the electron density map and allowed to refine isotropically. Friedel pairs were merged for the final refinement. The crystal data results are summarised in Tables 2 and 3.

### Thermal analysis and kinetics

Thermogravimetric analysis (TG) and differential scanning calorimetry (DSC) were performed on a Perkin Elmer 6 series system using a purge gas of nitrogen at 20 mL min<sup>−1</sup>. Experiments were conducted between 303–700 K at a heating rate of 10 K min<sup>−1</sup>. The crystals were removed from the mother liquor, dried on filter paper and crushed prior to analysis.

Kinetics of absorption: this was carried out with the aid of a special device, in which the powdered host compound is placed on an analytical balance and is enclosed in a chamber containing the volatile liquid guest and its vapours. The system is thermostated and the increase in mass with time was automatically recorded on a computer. The apparatus has been described in detail.<sup>17</sup> The vapour pressure of the amine was varied by preparing solutions of known mol fractions of the amine and water. A separate experiment confirmed that **H** does not absorb water. Ideal behaviour of the amine–water mixtures was assumed. The mass gain at 25 °C was recorded using ALPHATIME software.

Kinetics of desorption: non-isothermal kinetics<sup>18,19</sup> was performed on powdered samples formed directly from dissolution of **H** in the appropriate amine.

## Results and discussion

### Salts of achiral amines: structures

For all the structures proton transfer is observed from the carboxylic moiety of **H** to the nitrogen of the amine guest,

**Table 2** Crystal data parameters (salts of achiral guests)  $H = C_{24}H_{40}O_4$ 

Compound	$(H^-)(PPA^+) \cdot ACE$	$(2H^-)(2PPA^+) \cdot 4.3H_2O$	$(H^-)(DBA^+)$
Structural formula	$(H^-)(C_3H_{10}N^+) \cdot C_3H_6O$	$(2H^-)(2 C_3H_{10}N^+) \cdot 4.3H_2O$	$(H^-)(C_8H_{20}N^+)$
Molecular mass ( $g mol^{-1}$ )	509.75	980.47	521.8
Data collection temp. (K)	173(2)	173(2)	173(2)
Crystal system	Monoclinic	Triclinic	Monoclinic
Space group	$P2_1$	$P1$	$P2_1$
$a$ (Å)	11.0361(11)	7.7287(6)	14.043(3)
$b$ (Å)	7.7101(7)	11.5210(9)	7.8258(16)
$c$ (Å)	17.9654(18)	16.5589(13)	14.055(3)
$\alpha$ (°)	90.00	81.143(2)	90.00
$\beta$ (°)	105.750(2)	79.051(2)	100.94(3)
$\gamma$ (°)	90.00	89.485(2)	90.00
Volume (Å <sup>3</sup> )	1471.3(2)	1430.03(19)	1516.5(5)
$Z$	2	1	2
$D_c$ , Calc density ( $g cm^{-3}$ )	1.151	1.138	1.143
Absorption coefficient ( $mm^{-1}$ )	0.076	0.079	0.073
$F(000)$	564	542.7	580
$\theta$ range	1.92–28.31	2.03–28.38	1.48–28.29
Limiting indices	−14, 13; ±10; ±23	±10; −15, 12; −16, 22	±18; ±10; ±18
Reflections collected/unique	13 768/3922	11 575/7136	7058/4023
Goodness-of-fit on $F^2$	1.022	1.032	1.030
Final $R$ indices [ $I > 2\sigma(I)$ ]	$R_1 = 0.0408$ ; $wR_2 = 0.0950$	$R_1 = 0.0442$ ; $wR_2 = 0.1070$	$R_1 = 0.0413$ ; $wR_2 = 0.0941$
$R$ indices (all data)	$R_1 = 0.0554$ ; $wR_2 = 0.1023$	$R_1 = 0.0543$ ; $wR_2 = 0.1134$	$R_1 = 0.0633$ ; $wR_2 = 0.1028$
Largest diff. peak and hole ( $e \text{ \AA}^{-3}$ )	0.274; −0.203	0.308; −0.191	0.235; −0.198

forming salts. This is a classic interaction dependent on the difference in  $pK_a$  between the acid and the base.<sup>20</sup>

The hydrogen bonding found in  $(H^-)(PPA^+) \cdot ACE$  is shown in Fig. 2 and can be described with the graph set<sup>21</sup>  $N_1 = R_3^2(12)$ . It forms an infinite network running along the [010] direction. Fig. 3 shows the packing of the structure viewed along  $b$ . It is characterised by alternate layers of the host and the amine/acetone molecules. The amine cation is disordered, the major component refined with a site occupancy factor of 0.813. The acetone molecules are not involved in hydrogen bonding.

For  $(2H^-)(2PPA^+) \cdot 4.3H_2O$  the presence of water molecules results in extensive hydrogen bonding as can be seen in Fig. 4. The asymmetric unit contains two host molecules and two guest molecules, one of which is disordered. In addition, water molecules maintain a bridging role connecting neighbouring host molecules as well as linking H and PPA molecules to form a continuous network. The packing is shown in Fig. 5. This again displays double layers of the host where the lipophilic faces alternate with the hydrophilic faces. The water and amine guests bridge alternative hydrophilic layers of the host.

**Table 3** Crystal data (salts of chiral guests)  $H = C_{24}H_{40}O_4$ 

Compound	$(H^-)(R-BA^+)$	$(H^-)(S-BA^+)$	$(H^-)(R-MBA^+)$	$(H^-)(S-MBA^+)$
Structural formula	$(H^-)(C_4H_{12}N^+)$	$(H^-)(C_4H_{12}N^+)$	$(H^-)(C_5H_{14}N^+)$	$(H^-)(C_5H_{14}N^+)$
Molecular mass ( $g mol^{-1}$ )	465.70	465.70	479.72	479.72
Data collection temp. (K)	173(2)	173(2)	296 (2)	173(2)
Crystal system	Monoclinic	Monoclinic	Monoclinic	Monoclinic
Space group	$C2$	$P2_1$	$P2_1$	$P2_1$
$a$ (Å)	23.511(4)	10.1547(11)	11.501(2)	11.026(2)
$b$ (Å)	7.6318(12)	7.5678(8)	7.7042(15)	7.5245(15)
$c$ (Å)	18.196(3)	17.645(2)	17.175(3)	17.600(4)
$\alpha$ (°)	90.00	90.00	90.00	90.00
$\beta$ (°)	123.03(2)	90.915(3)	106.19(3)	105.26(3)
$\gamma$ (°)	90.00	90.00	90.00	90.00
Volume (Å <sup>3</sup> )	2737.3(10)	1355.8(5)	1461.5(5)	1408.7(5)
$Z$	4	2	2	2
$D_c$ , Calc density ( $g cm^{-3}$ )	1.130	1.141	1.090	1.131
Absorption coefficient ( $mm^{-1}$ )	0.074	0.074	0.071	0.073
$F(000)$	1032	516	532	532
$\theta$ range	1.74–26.39	2.01–28.32	1.84–25.63	2.51–25.30
Limiting indices	±29; ±9; ±22	±13; ±10; ±23	−14, 12; ±9; ±20	±13; ±9; ±21
Reflections collected/unique	10 356/3026	12 140/3604	8347/5311	5015/2760
Goodness-of-fit on $F^2$	1.050	1.024	1.006	0.964
Final $R$ indices [ $I > 2\sigma(I)$ ]	$R_1 = 0.0462$ ; $wR_2 = 0.1115$	$R_1 = 0.0403$ ; $wR_2 = 0.0986$	$R_1 = 0.0494$ ; $wR_2 = 0.1192$	$R_1 = 0.0425$ ; $wR_2 = 0.0869$
$R$ indices (all data)	$R_1 = 0.0663$ ; $wR_2 = 0.1222$	$R_1 = 0.0492$ ; $wR_2 = 0.1046$	$R_1 = 0.0869$ ; $wR_2 = 0.1380$	$R_1 = 0.0938$ ; $wR_2 = 0.0989$
Largest diff. peak and hole ( $e \text{ \AA}^{-3}$ )	0.364; −0.214	0.275; −0.171	0.199; −0.139	0.182; −0.183

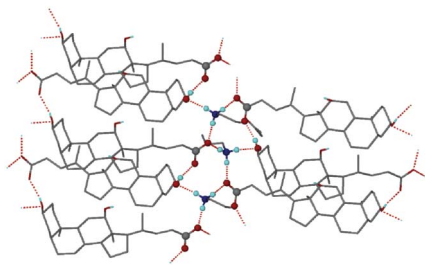


Fig. 2 Hydrogen bonding in  $(\text{H}^-)(\text{PPA}^+)\text{-ACE}$ .

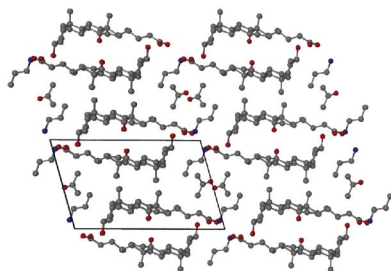


Fig. 3 Packing diagram of  $(\text{H}^-)(\text{PPA}^+)\text{-ACE}$  viewed down  $[010]$ .

For the  $(\text{H}^-)(\text{DBA}^+)$  structure, bifurcated hydrogen bonds connect two hosts to a DBA molecule. These repeating units are linked *via*  $(\text{Host})\text{COO}^- \cdots (\text{DBA})\text{HN}^+\text{H} \cdots \text{OOC}(\text{Host})$  hydrogen bonds which extend in an infinite chain along the  $[010]$  direction (Fig. 6). The DBA guests occupy voids in the  $(110)$  plane. The hydrogen bond results for all the structures have been tabulated in the ESI.†

#### Salts of chiral amines: structures

Crystals of  $(\text{H}^-)(\text{R-BA}^+)$  were obtained from a solution of the acid in racemic *sec*-butylamine. Thus, this resolution was successful in that no evidence of *S-BA*<sup>+</sup> was found in the crystal

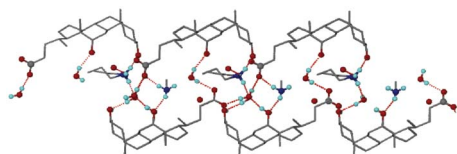


Fig. 4 Hydrogen bonding in  $(2\text{H}^-)(2\text{PPA}^+)\text{-}4.3\text{H}_2\text{O}$ .

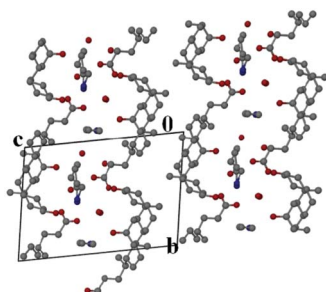


Fig. 5 Packing diagram of  $(2\text{H}^-)(2\text{PPA}^+)\text{-}4.3\text{H}_2\text{O}$  viewed down  $[100]$ .

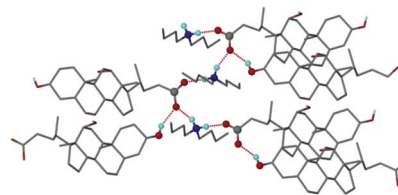


Fig. 6 Hydrogen bonding in  $(\text{H}^-)(\text{DBA}^+)$ .

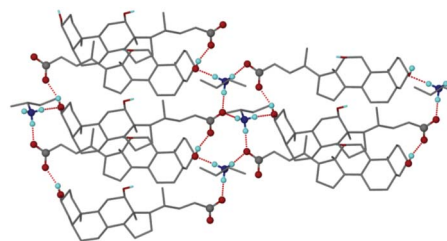


Fig. 7 Hydrogen bonding in  $(\text{H}^-)(\text{R-BA}^+)$ .

structure. The compound crystallises in the space group  $C2$  with  $Z = 4$ . The structure is stabilised by extensive hydrogen bonding and each N–H moiety of the amine ion acts as a donor either to a carboxylate oxygen or the hydroxyl oxygen of the host. This is shown in Fig. 7, which displays the ring nature of the hydrogen bonding scheme  $R_5^4(12)$ .

The compound  $(\text{H}^-)(\text{S-BA}^+)$  was crystallised directly from pure *S-BA* in the space group  $P2_1$  with  $Z = 2$ . The hydrogen bonding of this compound is analogous to that of its *R-BA* analogue. The crystal data for these compounds is given in Table 3. The packing of the two structures is different. Whereas pairs of  $\text{H}^-$  anions are related in their lipophilic faces by a diad screw axis in both structures, the lipophobic

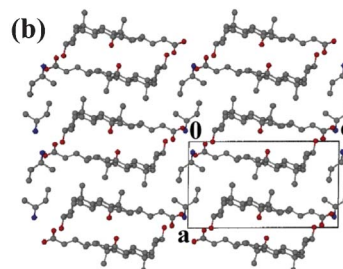
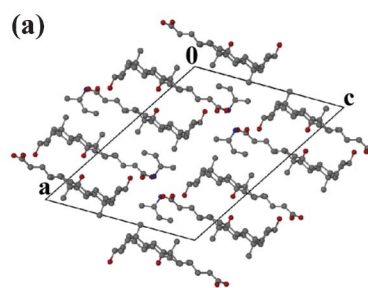


Fig. 8 Packing diagram of (a)  $(\text{H}^-)(\text{R-BA}^+)$  and (b)  $(\text{H}^-)(\text{S-BA}^+)$ .

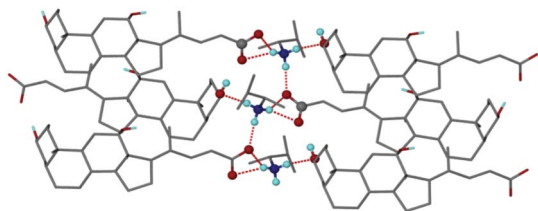


Fig. 9 Hydrogen bonding in  $(\text{H}^-)(\text{R-MBA}^+)$ .

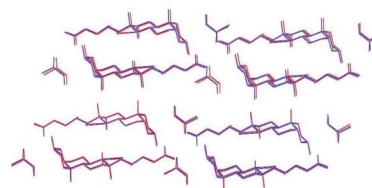


Fig. 10 Packing diagrams of  $(\text{H}^-)(\text{S-MBA}^+)$  in blue and  $(\text{H}^-)(\text{R-MBA}^+)$  in red, overlaid.

faces are related by a diad in the  $(\text{H}^-)(\text{R-BA}^+)$  structure (Fig. 8a) but by a two-fold screw axis in the  $(\text{H}^-)(\text{S-BA}^+)$  structure (Fig. 8b). This results in a relative shift of the hydrophobic faces of the host anions.

Both  $(\text{H}^-)(\text{R-MBA}^+)$  and  $(\text{H}^-)(\text{S-MBA}^+)$  crystallised in the space group  $P2_1$  with  $Z = 2$ . The data collection for the *R-MBA* compound was conducted at room temperature due to the crystal fracturing at low temperatures. A racemic mixture of *MBA* with the host resulted in the (*S*)-enantiomer being

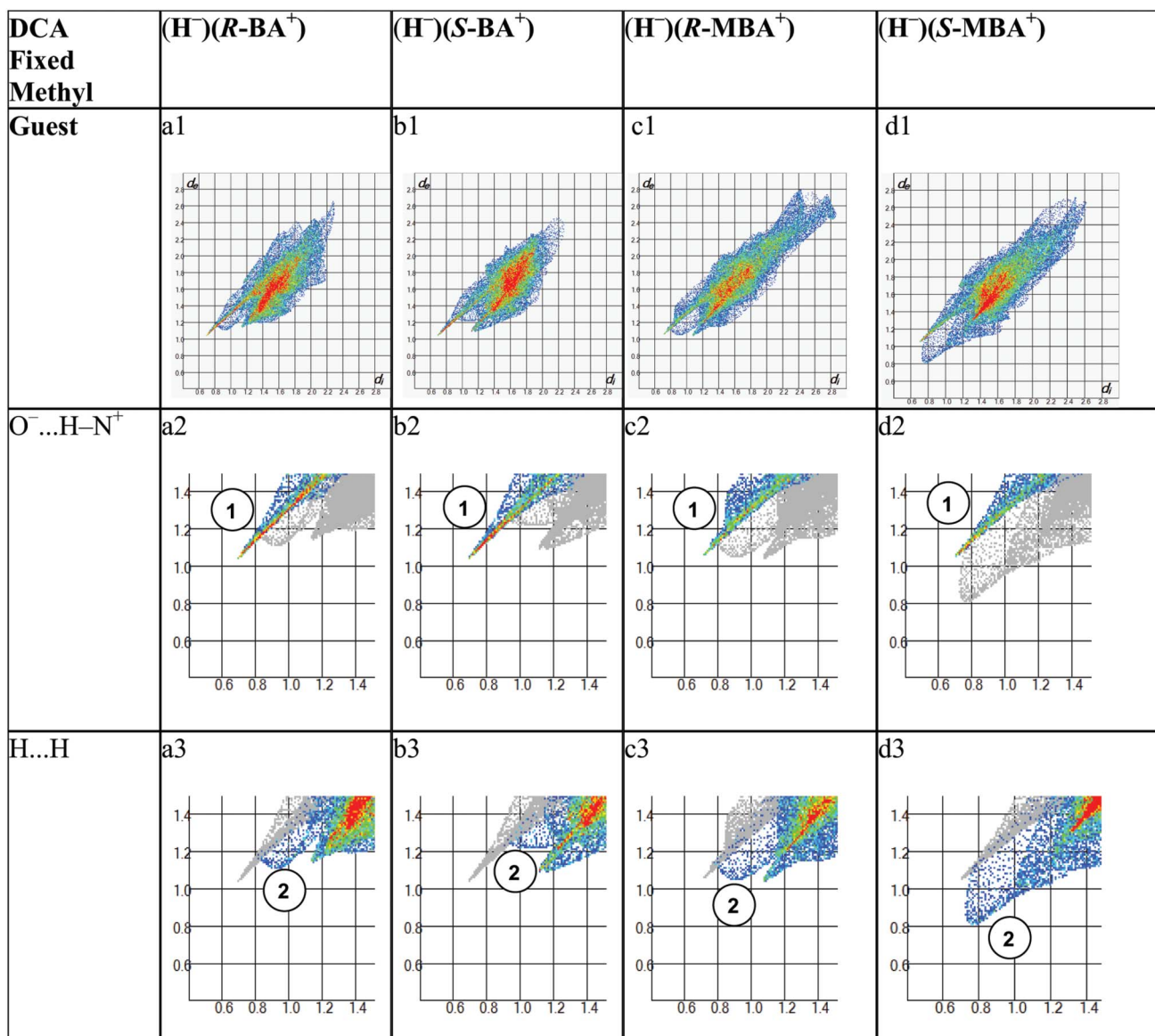


Fig. 11 Hirshfeld plots for a.  $(\text{H}^-)(\text{R-BA}^+)$ , b.  $(\text{H}^-)(\text{S-BA}^+)$ , c.  $(\text{H}^-)(\text{R-MBA}^+)$  and d.  $(\text{H}^-)(\text{S-MBA}^+)$ .

**Table 4** Hydrogen bonding (salts of chiral guests)

Compound	(H <sup>-</sup> )(R-BA <sup>+</sup> )	(H <sup>-</sup> )(S-BA <sup>+</sup> )	(H <sup>-</sup> )(R-MBA <sup>+</sup> )	(H <sup>-</sup> )(S-MBA <sup>+</sup> )
N1G...O3	2.890(3)	2.821(2)	2.878(3)	2.831(3)
N1G...O24A	2.752(3)	3.289(2)	2.990(4)	3.303(3)
N1G...O24A <sup>a</sup>	2.785(3)	2.730(2)	2.738(4)	2.724(3)
N1G...O24B	3.261(3)	2.785(2)	2.999(4)	2.763(3)

<sup>a</sup>: symmetry generated atom

chosen. For (H<sup>-</sup>)(R-MBA<sup>+</sup>) the NH<sub>3</sub><sup>+</sup> group acts a donor with each N–H bond involved in hydrogen bonding to either the carboxyl or hydroxyl functionality of neighbouring host molecules. Bifurcated bonds are also formed between the COO<sup>-</sup> of the host and the NH<sub>3</sub><sup>+</sup> group of the amine. This can be described by the graph set R<sub>5</sub><sup>3</sup>(10)R<sub>1</sub><sup>2</sup>(4). The hydrogen bonding is shown in Fig. 9.

The hydrogen bonding in the (H<sup>-</sup>)(S-MBA<sup>+</sup>) compound is analogous to that found in the R-MBA<sup>+</sup> structure. The packing diagrams for both structures have been overlaid to illustrate their similarity (Fig. 10).

### Resolution results

The salient point of the resolution experiment results is that the host, H, preferentially selects (*R*)-*sec*-butylamine (BA) or (*S*)-3-methyl-2-butylamine (MBA) from their respective racemic modifications. We therefore analysed the non-bonded interactions that impinge on each guest in the four structures. In order to be self consistent, the final refinements were carried out treating the –CH<sub>3</sub> and –NH<sub>3</sub><sup>+</sup> moieties as rigid groups with normalised *d*(C–H) and *d*(N–H) distances set at 1.08 Å. We employed the program Crystal Explorer, which calculates the Hirshfeld surfaces of a molecule in a crystal structure and depicts all the molecular interactions of the targeted molecule with its neighbours in the form of fingerprint plots.<sup>22</sup>

The results are shown in Fig. 11, which displays the fingerprint plots for each guest. The top row displays the maps of the complete set of interactions. In the second and third rows we highlight the close contacts where the sum of the internal and external distances are ≤ 2.8 Å. When comparing the (H<sup>-</sup>)(R-BA<sup>+</sup>) and (H<sup>-</sup>)(S-BA<sup>+</sup>) structures we note that the hydrogen bonds are very similar (Table 4): there are two strong hydrogen bonds and one weaker one in both structures. These are shown as spikes labelled 1 in Fig. 11a2 and b2. However, the H...H contacts of the guests shown in Fig. 11a3 and b3 and labelled 2, show significant differences. Fig. 11a3, for (H<sup>-</sup>)(R-BA<sup>+</sup>), shows more H...H interactions peaking at (de + di) = 1.11 + 0.90 = 2.01 Å, while Fig. 11b3 shows this interaction as 1.21 + 1.25 = 2.25 Å. This confirms a closer fit of the carbon-bound hydrogens of the R-BA<sup>+</sup> guest with the surrounding host surface. This feature is even more pronounced in the case of the (H<sup>-</sup>)(R-MBA<sup>+</sup>) and (H<sup>-</sup>)(S-MBA<sup>+</sup>) structures. We again have similar O<sup>-</sup>...H–N<sup>+</sup> hydrogen bonds (Table 4), displayed as spikes labelled 1 in Fig. 11c2 and d2, but the H...H interactions are strongly different. In Fig. 11d3, the peak labelled 2 occurs at (de + di) = 1.56 Å, much closer than that in Fig. 11c3 at 1.95 Å.

Interestingly, a grinding experiment whereby a few drops of racemic *sec*-butylamine was added to H (ground for a few minutes) resulted in the kinetically preferred (H<sup>-</sup>)(S-BA<sup>+</sup>). This is in contrast to the thermodynamically stable product (H<sup>-</sup>)(R-BA<sup>+</sup>) obtained upon slow stirring a 1 : 1 mixture of H and racemic *sec*-butylamine, which is identical to that obtained by slow evaporation of the solution that yielded single crystals. The powder X-ray diffraction results are shown in Fig. 12. An analogous experiment could not be carried out with racemic 3-methyl-2-butylamine due to the similarity between the calculated powder patterns<sup>23</sup> of (H<sup>-</sup>)(R-MBA<sup>+</sup>) and (H<sup>-</sup>)(S-MBA<sup>+</sup>).

### Thermal analysis and kinetics

The results of the TG and DSC analyses are summarised in Tables 5 and 6. For the decomposition of (H<sup>-</sup>)(PPA<sup>+</sup>)·ACE the mass loss observed is due to the release of the PPA guest (calculated 13.1%). The acetone evaporated prior to analysis. This is in accordance with the structural results where the acetone occupies channels and is not involved in hydrogen bonding. A single broad endotherm corresponds to guest loss and concomitant host melt.

For (2H<sup>-</sup>)(2PPA<sup>+</sup>)·4.3H<sub>2</sub>O the loss of water is followed by the release of PPA (total calculated 20.0%) and the host melt. This is depicted by three endotherms in the DSC. The loss of DBA in (H<sup>-</sup>)(DBA<sup>+</sup>) is shown by a single mass loss step in the TG.

A complex endotherm in the DSC curve is due to the release of DBA and the host melt. For all three structures decomposition was observed after 600 K. The endotherm associated with

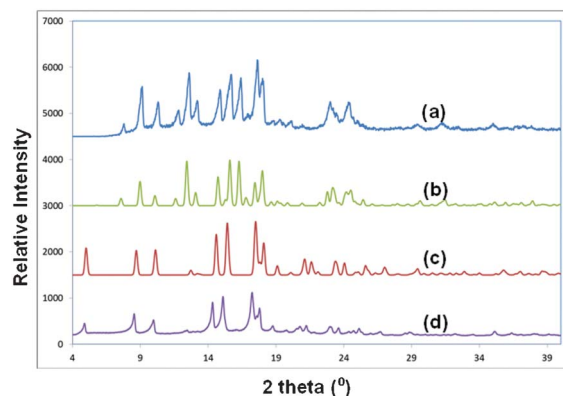


**Fig. 12** PXRD patterns of (a) (H<sup>-</sup>)(R-BA<sup>+</sup>) obtained from stirring, (b) calculated (H<sup>-</sup>)(R-BA<sup>+</sup>), (c) calculated (H<sup>-</sup>)(S-BA<sup>+</sup>) and (d) (H<sup>-</sup>)(S-BA<sup>+</sup>) obtained from grinding.

**Table 5** Thermal analysis results (salts of achiral guests)

Compound	(H <sup>-</sup> )(PPA <sup>+</sup> )-ACE	(2H <sup>-</sup> )(2PPA <sup>+</sup> )-4.3H <sub>2</sub> O	(H <sup>-</sup> )(DBA <sup>+</sup> )
H : G ratio	1 : 1 : 1	2 : 2 : 4.3	1 : 1
TG (calc % mass loss)	13.1	20.0	24.8
TG (exp % mass loss)	11.9	18.8	25.7
DSC endotherm range (T/K)	400–480	330–410 (H <sub>2</sub> O) 410–480 (PPA)	380–480
	—		—

**Table 6** Thermal analysis data (salts of chiral guests)

Compound	(H <sup>-</sup> )(R-BA <sup>+</sup> )	(H <sup>-</sup> )(S-BA <sup>+</sup> )	(H <sup>-</sup> )(R-MBA <sup>+</sup> )	(H <sup>-</sup> )(S-MBA <sup>+</sup> )
H : G ratio	1 : 1	1 : 1	1 : 1	1 : 1
TG (calc % mass loss)	15.7	15.7	18.4	18.4
TG (exp % mass loss)	15.7	15.3	17.8	17.8
DSC endotherm range (T/K)	406–478	395–509	405–495	412–503

the loss of the BA guest and the concomitant dissolution of the host is diffuse. We note that the onset temperature for (H<sup>-</sup>)(R-BA<sup>+</sup>) is 406 K, which is 11 K higher than that of the (H<sup>-</sup>)(S-BA<sup>+</sup>) analogue. This is a measure of the higher stability of the former compound and serves as an indication of why the *R*-enantiomer is selected by the host from the racemic modification. A similar thermal profile was found for (H<sup>-</sup>)(R-MBA<sup>+</sup>) and (H<sup>-</sup>)(S-MBA<sup>+</sup>) as illustrated in Fig. 13. The higher onset temperature for the *S*-MBA<sup>+</sup> compound illustrates the greater stability of (H<sup>-</sup>)(S-MBA<sup>+</sup>).

### Kinetics of salt formation

Kinetics of absorption were performed with the guests PPA and racemic BA. Experiments were conducted at 298 K with varying vapour pressure as described above. The resultant salts formed were hygroscopic and absorbed greater quantities of

amine than the stoichiometrically calculated amounts. The resultant curves were linear after the absorption of the stoichiometrically expected amount of amine. The linear curve is indicative of a zero order reaction and in this example is dependent on the surface area of the salt exposed to the amine vapour. The curves were analysed until the end of the expected mass gain with a molar ratio of 1 : 1 (H : amine). The mass gain data were converted to the extent of the reaction:

$$\alpha = \frac{m_t - m_0}{m_\infty - m_0}$$

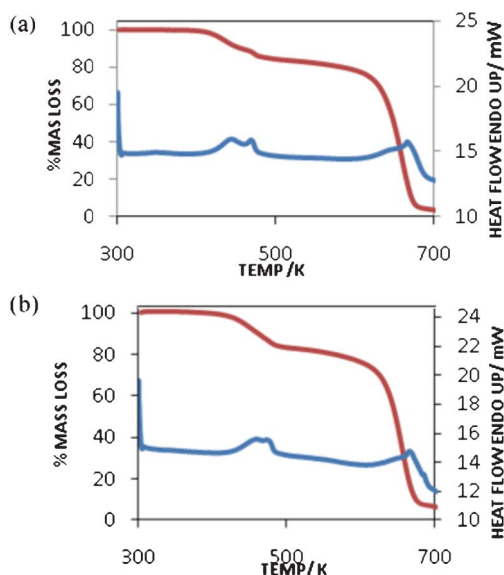
where  $m_0$ ,  $m_t$  and  $m_\infty$  are the recorded masses at the start, during and at the end of the experiment.

The rate of the reaction can be described by:

$$\frac{d\alpha}{dt} = k_{\text{obs}}f(\alpha)$$

where  $k_{\text{obs}}$  is the observed rate constant. Several models for the kinetics are applicable and are based on various assumptions: nucleation, geometrical contraction, diffusion and reaction order. In the case of the reaction under study, the deceleratory geometric model R2 (contracting area):

$$[1 - (1 - \alpha)^2] = k_{\text{obs}}t$$

**Fig. 13** TG and DSC profiles for (a) (H<sup>-</sup>)(R-MBA<sup>+</sup>) and (b) (H<sup>-</sup>)(S-MBA<sup>+</sup>).**Table 7** Kinetics of absorption results

Amine	$X_{\text{amine}}$	$P_{\text{amine}}/\text{mmHg}$	Slope $k_{\text{obs}}/\text{min}^{-1}$	$R$
PPA	1	310.0	1.460	0.9914
	0.5	155.0	0.750	0.9984
	0.30	93.9	0.504	0.9966
	0.25	77.5	0.436	0.9904
	0.17	51.6	0.327	0.9979
Racemic BA	1	178	0.519	0.9953
	0.5	89.0	0.217	0.9920
	0.30	53.4	0.183	0.9951
	0.25	44.5	0.164	0.9970
	0.17	29.7	0.086	0.9992

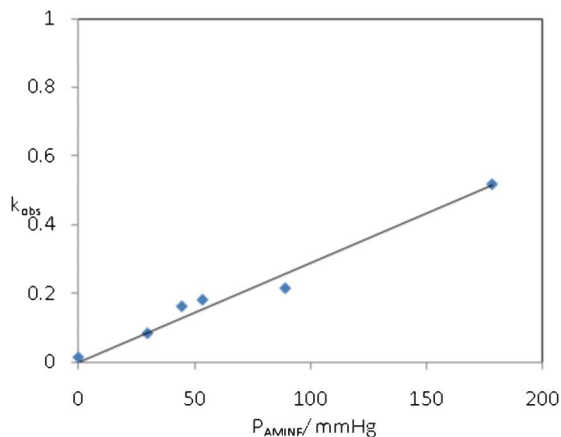


Fig. 14 Plot of  $k_{\text{obs}}$  vs.  $P_{\text{amine}}$  where the blue diamonds indicate the absorption of racemic BA.

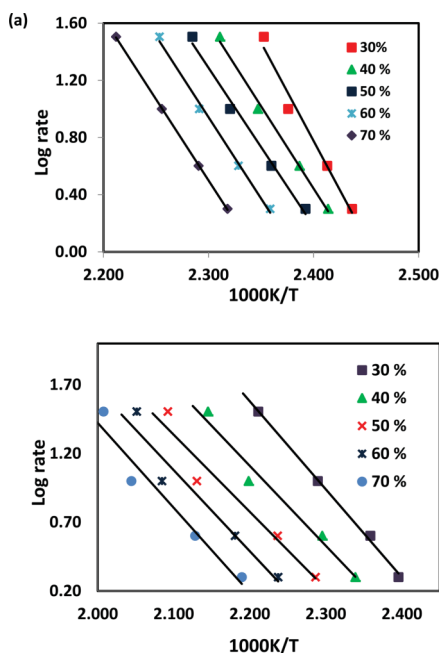


Fig. 15  $\log \beta$  vs.  $1/T$  plot for the decomposition of (a)  $\text{H}^-\text{BA}^+$  and (b)  $\text{H}^-\text{DBA}^+$ .

fitted all the data ( $\alpha = 0.05$ – $0.75$  for PPA and  $\alpha = 0.05$ – $0.90$  for BA). The  $k_{\text{obs}}$  values clearly depend on the vapour pressure of the amine which was controlled by diluting to various mole fractions with water. The results are given in Table 7.

The observed rate constant depends on the vapour pressure of the amine. Thus,  $k_{\text{obs}} = kP_{\text{amine}}$ . A plot of  $k_{\text{obs}}$  vs. vapour pressure is shown in Fig. 14. For the absorption of PPA:  $k = 4.6 \times 10^{-3} \text{ min}^{-1} \text{ mmHg}^{-1}$  and for racemic BA:  $k = 2.8 \times 10^{-3} \text{ min}^{-1} \text{ mmHg}^{-1}$

#### Kinetics of salt decomposition

Powdered samples of  $\text{H}^-\text{BA}^+$  and of  $\text{H}^-\text{DBA}^+$  were prepared by direct addition of the respective amines to the dry host powder. The decomposition of these salts was monitored by TG using non-isothermal kinetics. TG experiments were

completed at heating rates 2, 4, 10 and  $32 \text{ K min}^{-1}$ . The resultant % mass loss vs. temperature curves were converted into  $\alpha$  vs. temperature curves. The data was analysed in the range  $\alpha = 0.3$ – $0.7$ . Plots of  $\log \beta$  vs.  $1/T$  where  $\beta$  is the heating rate are given in Fig. 15.

The activation energies were calculated using the relationship

$$\text{slope} = -0.457 \frac{E_a}{R}$$

For  $\text{H}^-\text{BA}^+$  the activation energy range was 201.6–250.1  $\text{kJ mol}^{-1}$  and for  $\text{H}^-\text{DBA}^+$  the activation energy was calculated as 101.9–116.4  $\text{kJ mol}^{-1}$ .

## Conclusion

(+)-Deoxycholic acid forms salts with the achiral and chiral amines studied, *via* proton transfer from the carboxylic moiety of the host to the nitrogen of the amine guest. We achieved diastereomeric resolution of racemic mixtures of *sec*-butylamine and 3-methyl-2-butylamine. Crystallisation of racemic *sec*-butylamine and (+)-deoxycholic acid gave the (*R*)-enantiomer in the crystal structure. An analogous experiment with racemic 3-methyl-2-butylamine yielded exclusively crystals containing the (*S*)-enantiomer. The structures obtained from crystallisation of (+)-deoxycholic acid in (*R*)-*sec*-butylamine and (*S*)-*sec*-butylamine, respectively, were analysed and indicated similar hydrogen bonding patterns but significant differences in the  $\text{H}\cdots\text{H}$  interactions. A similar result was seen for experiments with 3-methyl-2-butylamine. We have thus successfully correlated the resolution results with the non-bonded interactions in the crystal structures. The sensitivity of the chiral discrimination process is further demonstrated by the grinding experiment of (+)-deoxycholic acid and racemic *sec*-butylamine where the (*S*)-*sec*-butylamine was selected, indicating the importance of reaction conditions on the resolution.

## Acknowledgements

We thank the Cape Peninsula University of Technology for funding.

## References

- 1 S. Budavari, M. J. O'Neal, A. Smith, P. E. Heckelman and J. F. Kinneary in *The Merck Index: An Encyclopedia of Chemicals, Drugs, and Biologicals*, Merck & Co., Inc., Whitehouse Station, NJ, 12th edn, 1996.
- 2 E. Giglio, in *Inclusion Compounds*, ed. J. L. Atwood, J. E. D. Davies and D. D. MacNicol, Academic Press, London, 1984, vol. 2.
- 3 M. Miyata and K. Sada, in *Comprehensive Supramolecular Chemistry*, ed. D. D. MacNicol, F. Toda and R. Bishop, Elsevier, Oxford, 1996, vol. 6.

- 4 M. Miyata, K. Sada and N. Yoswathananont, *Encyclopedia of Supramolecular Chemistry*, ed. J. L. Atwood and J. W. Steed, Marcel Dekker, New York, 2004, p. 441.
- 5 O. Bortolini, G. Fantin and M. Fogagnolo, *Chirality*, 2010, **22**, 486.
- 6 L. R. Nassimbeni, N. B. Báthori and T.-L. Curtin, *Cryst. Growth Des.*, 2012, **12**, 4144–4148.
- 7 D. J. Collins and J. J. Hobbs, *Aust. J. Chem.*, 1970, **23**, 119.
- 8 R. C. Kelly, I. Schletter, S. J. Stein and W. Wierenga, *J. Am. Chem. Soc.*, 1979, **101**, 1054.
- 9 M. I. M. Tahir, N. H. Rees, S. J. Heyes, A. R. Cowley and K. Prout, *Chirality*, 2008, **20**, 863.
- 10 H. Wu and H. G. Jones, *Chem. Eng. Technol.*, 2012, **35**, 1031.
- 11 COLLECT, Data Collection Software, Nonius, Delft, The Netherlands, 1998.
- 12 APEX 2, version 1.0–27, Bruker AXS Inc., Madison, Wisconsin, USA, 2005.
- 13 Z. Otwinowski and W. Minor in *Methods in Enzymology, Macromolecular Crystallography*, ed. C. W. Carter Jr and R. M. Sweet, Academic Press, 1997, **vol. 276**, p. 307.
- 14 *SAINT-Plus*, Version 7.12, Bruker AXS Inc., Madison, Wisconsin, USA, 2004.
- 15 G. M. Sheldrick, *SHELX-97, Program for Crystal Structure Refinement*, University of Göttingen, Germany, 1997.
- 16 L. J. Barbour, X-Seed – a software tool for supramolecular crystallography, *J. Supramol. Chem.*, 2001, **1**, 189.
- 17 L. R. Nassimbeni, H. Su and T. L. Curtin, *Supramol. Chem.*, 2012, **24**, 344.
- 18 J. H. Flynn and L. A. Wall, *J. Polym. Sci., Part B: Polym. Lett.*, 1966, **4**, 323.
- 19 T. Ozawa, *Bull. Chem. Soc. Jpn.*, 1965, **38**, 1881.
- 20 S. L. Childs, G. P. Stahly and A. Park, *Mol. Pharmaceutics*, 2007, **4**, 323.
- 21 M. C. Etter, J. C. MacDonald and J. Bernstein, *Acta Crystallogr., Sect. B: Struct. Sci.*, 1990, **46**, 256.
- 22 M. A. Spackman and J. J. McKinnon, *CrystEngComm*, 2002, **4**, 378.
- 23 K. Yvon, W. Jeitschko and E. Parthè, LAZY PULVERIX – a computer program for calculating X-ray and neutron diffraction powder patterns, *J. Appl. Crystallogr.*, 1977, **10**, 73.